Applied Surface Science 256 (2010) 3546–3553

Contents lists available at ScienceDirect

Applied Surface Science

journal homepage: www.elsevier.com/locate/apsusc

Properties of mesoporous tungstosilicic acid/titania composites prepared by sol–gel method

Mirta N. Blanco, Luis R. Pizzio *

Centro de Investigación y Desarrollo en Ciencias Aplicadas "Dr. J. J. Ronco" (CINDECA), Departamento de Química, Facultad de Ciencias Exactas, UNLP-CCT La Plata, CONICET, 47 N° 257, 1900 La Plata, Argentina

ARTICLE INFO

Article history:
Received 11 November 2009
Received in revised form 18 December 2009
Accepted 22 December 2009
Available online 4 January 2010

Keywords:
Titania
Tungstosilicic acid
Urea template
Mesoporous solid

ABSTRACT

The tungstosilicic acid/titania composites were prepared by the sol–gel method. Titanium isopropoxide was used as titania precursor, and urea as a low-cost template. The tungstosilicic acid (TSA) was added in the same step as that in which titania hydrogel is formed. The TSA-modified samples only showed the characteristic peaks of anatase phase of titanium oxide in the XRD patterns, indicating that the presence of TSA retarded the crystallization of the anatase phase and its transformation into the rutile phase. Spherical particles with sizes between 200 and 700 nm, formed by aggregation of nanoparticle aggregates (4–50 nm in size), were observed. The particle size increased when the TSA content was raised and also increased slightly with the thermal treatment temperature. Mesoporous materials were obtained, with a mean pore diameter higher than 3.1 nm. Both the increase of the TSA concentration in the solid and the calcination temperature led to a decrease in the specific surface area of the samples. The main heteropolyoxometallate species present in the composites is the $[SiW_{12}O_{40}]^{4-}$ anion for the composites calcined up to 500 °C. The *band gap* energy decreased as a result of the introduction of TSA into the titania matrix, though it remained almost constant with the calcination temperature increase.
© 2010 Elsevier B.V. All rights reserved.

1. Introduction

Titanium dioxide (titania) is a material widely used as photocatalyst because it has a relatively high chemical stability, a negligible toxicity, a low cost, and it is easily available. Titania performance in the photodegradation of contaminants contained in wastes is influenced by the crystal structure, the crystallinity, the surface area, the porosity, the surface hydroxyl density, and the *band gap* energy [1–3], among other factors.

A low surface area and the hole–electron recombination are the main effects that can lead to a low photocatalytic activity. So, an increase in the surface area and the separation of electrons and holes can improve the photocatalytic activity of titania. Sol–gel reactions using urea as a low-cost pore-forming agent were found to be a good method to synthesize mesoporous titania with suitable properties to be used as a photocatalyst [4,5].

The doping of semiconductors with certain metal ions can help to extend the light absorption of large *band gap* semiconductors to the visible region, as reported by Anpo [6]. Particularly, the transition metal ions can lead to this *band gap* shift when they are impregnated on these semiconductors, allowing the use of light from the visible region of the spectrum. Furthermore, the transition metals or metal oxides may act as electron trappers, thus avoiding the recombination of the electron–hole pairs of titania-based catalysts [7–11].

Though heteropolyoxometallates (POMs) are widely used as oxidation as well as acid catalysts [12,13], they can also be effective homogeneous photocatalysts in the oxidation of organic compounds [14] and in the degradation of organic pollutants in water [15,16].

So, some POMs have been employed as titania modifiers intending to reduce the charge recombination. Another advantage of the incorporation of POMs into the titania matrix is the improvement of the catalyst density, which facilitates the catalyst separation from heterogeneous reaction and allows the catalyst reuse [17].

POMs have been added to TiO_2 suspensions [18], incorporated into TiO_2 colloids [19], or anchored to TiO_2 by chemical interactions [20]. Unlike these researchers, who have modified the surface of previously prepared TiO_2 with POMs, we studied the incorporation of tungstophosphoric acid into the titania matrix during the TiO_2 gel synthesis, in a similar way to Li et al. [17], but using urea as low-cost template with the purpose of obtaining mesoporous materials [21]. As a continuation of this previous work, we now study the preparation and characterization of tungstosilicic acid (TSA)/mesoporous titania composites synthesized via HCl-catalyzed sol–gel reactions, where urea is used as a low-cost pore-forming agent. To the best of our knowledge, this is the first time that these materials have been successfully synthesized in only one

* Corresponding author. Fax: +54 221 4211353.
E-mail address: lrpizzio@quimica.unlp.edu.ar (L.R. Pizzio).

0169-4332/$ – see front matter © 2010 Elsevier B.V. All rights reserved.
doi:10.1016/j.apsusc.2009.12.105

preparation step. The aim is to study the influence of some preparation conditions, such as the TSA concentration and the calcination temperature, on the characteristics attained in the materials designed to be used as photodegradation catalysts.

2. Experimental

2.1. Sample preparation

Firstly, titanium isopropoxide (Aldrich, 26.7 g) was mixed with absolute ethanol (Merck, 186.6 g), and stirred under N_2 at room temperature (r.t.) for 10 min, in order to obtain a homogeneous solution. Then, a 0.28 M HCl aqueous solution (0.33 cm^3) was slowly added to catalyze the sol–gel reaction. Afterwards, a urea–alcohol–water solution (120 g) in a 1:5:1 weight ratio was added to the hydrolyzed solution to act as template, together with an ethanol solution of $H_4SiW_{12}O_{40}{\cdot}23H_2O$ (Fluka p.a.), under constant stirring. The appropriate TSA solution concentrations in order to obtain a TSA amount of 0, 10, 20 and 30% by weight in the final material were used. The samples will be named TiTSA00, TiTSA10, TiTSA20, and TiTSA30, respectively. The gels were subsequently kept in a beaker till dryness. The obtained materials were ground into powder, and then extracted with distilled water for three periods of 24 h, in a system with continuous stirring, to remove urea. For all the samples, the tungsten amount in the solution obtained after the extraction step, determined by atomic absorption spectrometry, was lower than 4% of the total amount of TSA used. The solids were finally thermally treated at 100, 200, 300, 400, 500, and 600 °C for 2 h, and will be hereinafter named $TiTSAXX_{T100}$, $TiTSAXX_{T200}$, $TiTSAXX_{T300}$, $TiTSAXX_{T400}$, $TiTSAXX_{T500}$, and $TiTSAXX_{T600}$, respectively, where XX is the TSA concentration.

2.2. Solid characterization

Powder X-ray diffraction (XRD) patterns were obtained using Philips PW-1732 diffractometer with built-in recorder, using Cu Kα radiation, nickel filter, 20 mA and 40 kV in the high voltage source, scanning angle between 5° and 60° 2θ, and scanning rate of 1°/min.

The solids were studied by transmission electron microscopy (TEM) in a JEOL 100 CXII microscope, working at 100 kV and at a magnification of 80,000×. The samples were crushed in an agate mortar, ultrasonically dispersed in isobutanol, and deposited on a carbon-coated copper grid. The particle size distribution of the samples was determined by manual image analysis of a few hundred particles.

The secondary electron micrographs of the samples were obtained by scanning electron microscopy (SEM), using Philips Model 505 equipment.

The specific surface area, the pore volume and the mean pore size of the solids were determined from N_2 adsorption–desorption isotherms at −196 °C, obtained using Micromeritics ASAP 2020 equipment, with samples previously degassed at 100 °C for 2 h.

The thermogravimetric analysis (TGA) and the differential scanning calorimetry (DSC) measurements of the samples were performed with Shimadzu DT 50 thermal analyzer. Both analyses were carried out under argon, using 20–30 mg sample weight and a heating rate of 10 °C/min, in the temperature range 20–700 °C.

The Fourier transform infrared (FT-IR) spectra of the synthesized materials were obtained with Bruker IFS 66 FT-IR spectrometer and pellets in KBr, in the wavenumber range 400–4000 cm^{-1}.

The point of zero charge (pH_{PZC}) of each sample was estimated using the mass titration method proposed by Noh and Schwarz [22]. Suspensions of the solid in deionized water ranging from 0.01 to 20% w/w were prepared and the pH measured after stirring for 24 h.

By UV–vis diffuse reflectance spectroscopy (DRS), the spectra of the solids were recorded using a Lambda 35 PerkinElmer spectrophotometer, to which a diffuse reflectance chamber with a 50 mm diameter integrating sphere and internal Spectralon coating was attached. The measured range was 200–800 nm.

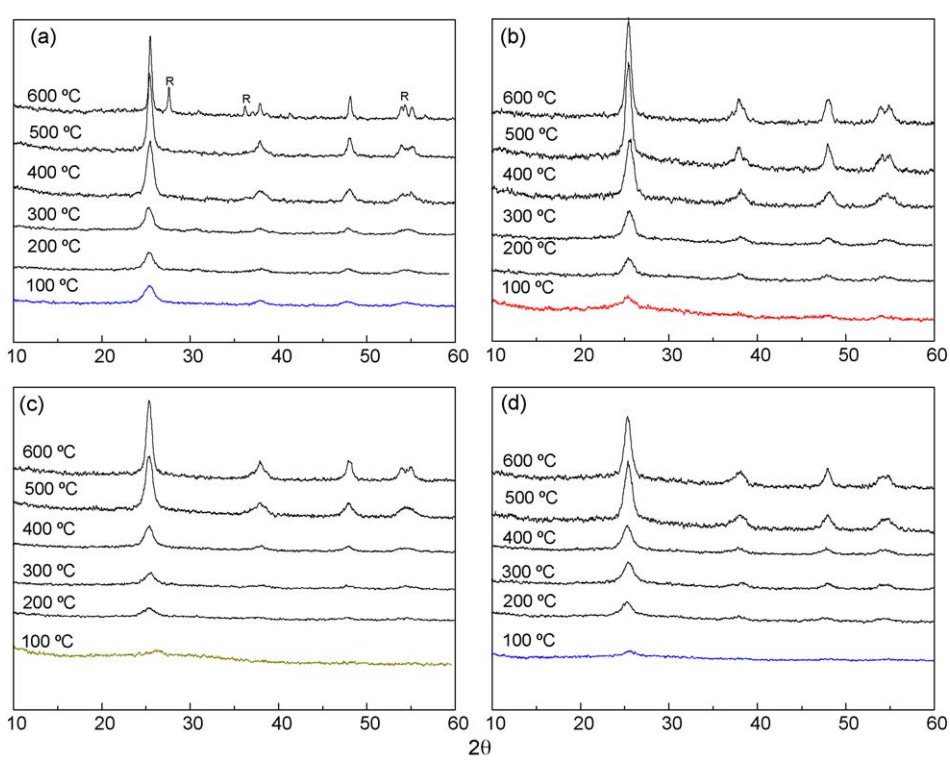

Fig. 1. XRD patterns of TiTSA00 (a), TiTSA10 (b), TiTSA20 (c), and TiTSA30 (d) samples, treated at different temperatures (R = peaks assigned to rutile phase).

3. Results and discussion

The XRD pattern of $TiTSA00_{T100}$, $TiTSA00_{T200}$, and $TiTSA00_{T300}$ samples (Fig. 1a) showed weak broad peaks in the same position where the characteristic peaks of the anatase phase are placed: 25.3° (1 0 1), 37.9° (0 0 4), 47.8° (2 0 0), and 54.3° 2θ. This is indicative of a solid poorly crystallized and mostly amorphous. The intensity of the peaks became stronger with the calcination temperature rise, which was better seen for the peak at 25.3° 2θ. The crystallinity of the TiTSA00 sample increased when the temperature was raised, and the peak at 54.3° splits into two peaks at 54.0° (1 0 5) and 54.9° (2 1 1) when the temperature was above 300 °C ($TiTSA00_{T400}$ and $TiTSA00_{T500}$ samples). At 600 °C, the XRD pattern exhibited three new peaks at 2θ = 27.4°, 36.1°, and 54.2°, indicating that a partial transformation of anatase into rutile phase occurred in the $TiTSA00_{T600}$ sample.

All the samples modified with TSA, including the $TiTSA10_{T600}$, $TiTSA20_{T600}$, and $TiTSA30_{T600}$ samples (Fig. 1b), only showed the presence of titania in anatase structure, suggesting that the anatase into rutile phase transition is shifted to higher temperatures in the presence of TSA. The results indicate that titania crystallization is retarded, and the anatase phase is stabilized, as was reported when other additives were added [23,24]. The crystallinity degree of the TSA/titania composites increased with the calcination temperature, but to a lower extent for higher TSA amount. Neither crystalline TSA nor TSA decomposition products were observed by XRD, so TSA could be well dispersed in the titania matrix or crystallites low enough to be detected by this technique could be present.

The anatase crystallite size (D_C) of samples thermally treated at 100 °C, estimated from the XRD results using the Scherrer equation and silicon as standard for the correction of instrumental broadening, showed that D_C is almost independent of the TSA content (Table 1). However, a D_C increase for higher calcination temperatures was observed, though the increment was lower for higher TSA content. This behavior may be attributed to crystal growth delay, which is very common in materials containing both a crystalline and an amorphous phase [25].

The particle size distribution obtained from TEM for the $TiTSA00_{T100}$, $TiTSA10_{T100}$, $TiTSA20_{T100}$, and $TiTSA30_{T100}$ samples is shown in Fig. 2. As can be seen, the mean particle size (D_M) and the standard deviation (σ) increase with the increment of TSA content. The particles displayed a size distribution between 4 and 50 nm.

Taking into account the D_C values estimated using the Scherrer equation, it can be suggested that these particles are formed by the agglomeration of small primary particles (approximately 5 nm in size). These results are in agreement with those published by Carriazo et al. [26] for commercial titania samples impregnated with tungstophosphoric acid. The size of the agglomerates increased when both the TSA concentration in the solid and the thermal treatment temperature were higher.

The SEM micrographs of the samples thermally treated at 100 °C, shown in Fig. 3, revealed that titania samples consist of spherical particles, whose size increases from 200 to 700 nm when the TSA content is raised. These spherical particles seem to be formed by aggregation of the nanoparticle agglomerates, as was reported by Bakardjieva et al. [27] for titania samples obtained by hydrolysis of $TiOSO_4$ aqueous solution using urea as the precipitation agent. The size and shape of the spherical particles remain practically unchanged during the calcination step. However, these particles formed clusters and, while for the TiTSA00 and TiTSA10 samples the cluster size increased slightly for higher thermal treatment temperatures, this process was negligible for the TiTSA20 and TiTSA30 samples.

The textural properties of the samples were estimated from the N_2 adsorption–desorption isotherms (Fig. 4). The TSA/titania composites displayed isotherms classified as type IV, characteristic of mesoporous materials. The hysteresis loop of TSA-modified titania samples (H2 type) was slightly higher than that of TiTSA00.

The specific surface area (S_{BET}) was determined using the Brunauer–Emmett–Teller (BET) method, the specific surface area of micropores (S_{micro}) was estimated by the *t*-plot method, and the total pore volume and the average pore diameter (D_p) were obtained using the Barret–Joyner–Halenda (BJH) method. The results for the TiTSA00 and the TSA/titania composites calcined at 100 °C are shown in Table 1.

The samples are mesoporous materials with a D_p higher than 3.1 nm. The S_{BET} decreased and the D_p increased for higher TSA concentration in the solid. Taking into account the values of S_{micro}, less than 10% of the total specific surface area is due to a microporous structure.

S_{BET} decreased according to the following order: $TiTSA00_{T100} > TiTSA10_{T100} > TiTSA20_{T100} > TiTSA30_{T100}$ (Table 1), which may be related to a lower cross-linking degree caused by the acid concentration increase. A similar behavior for the specific surface of mesoporous titania obtained via the sol–gel process to those previously reported using hydrochloric or acetic acids was observed [28,29].

S_{BET} varied when the calcination temperature was increased, as is shown in Fig. 5. For titania without TSA addition, S_{BET} decreased almost 60% when the calcination temperature was raised from 100 to 200 °C, but the decrease was significantly lower for the TSA/titania composites. It was 28% for TiTSA10, 8% for TiTSA20, and only 1% for TiTSA30 samples. This could be attributed to the interaction of the TSA incorporated into titania, which can reduce the agglomeration by surface diffusion and/or sintering [23,30,31]. Besides, similar S_{BET} values were found for TiTSA20 and TiTSA30 samples treated at higher temperatures. This result could indicate a limiting value for the above-mentioned TSA–titania interaction.

An electrostatic interaction between TSA and titania can be assumed, caused by transfer of protons to Ti–OH groups. During the thermal treatment, water is released from the [Ti–OH_2^+] group, and a direct bonding of the polyanion to titania is induced [32]. Nevertheless, the adsorption might not be purely electrostatic. It can also involve hydrogen-bond type interactions between oxygen atoms of TSA species and hydroxyl groups of titania.

Table 1
Physicochemical properties of the TSA-modified mesoporous titania treated at 100 °C.

Sample	S_{BET} (m^2/g)	S_{micro}[a] (m^2/g)	D_p[b] (nm)	Total pore volume[c] (cm^3/g)	D_C[d] (nm)	N_w[e]	OH/nm^2
$TiTSA00_{T100}$	372	35	3.1	0.195	5.9	1.35×10^{21}	7.3
$TiTSA10_{T100}$	238	18	4.2	0.215	5.5	0.85×10^{21}	7.1
$TiTSA20_{T100}$	208	15	4.8	0.166	5.5	0.76×10^{21}	7.3
$TiTSA30_{T100}$	160	12	5.0	0.104	5.6	0.61×10^{21}	7.6

[a] Specific surface area of micropores was obtained from *t*-plot analysis.
[b] Average pore diameter was calculated using the BJH formula from the desorption branch.
[c] Total pore volume was calculated by the BJH method.
[d] Anatase crystallite size.
[e] Number of water molecules released per gram.

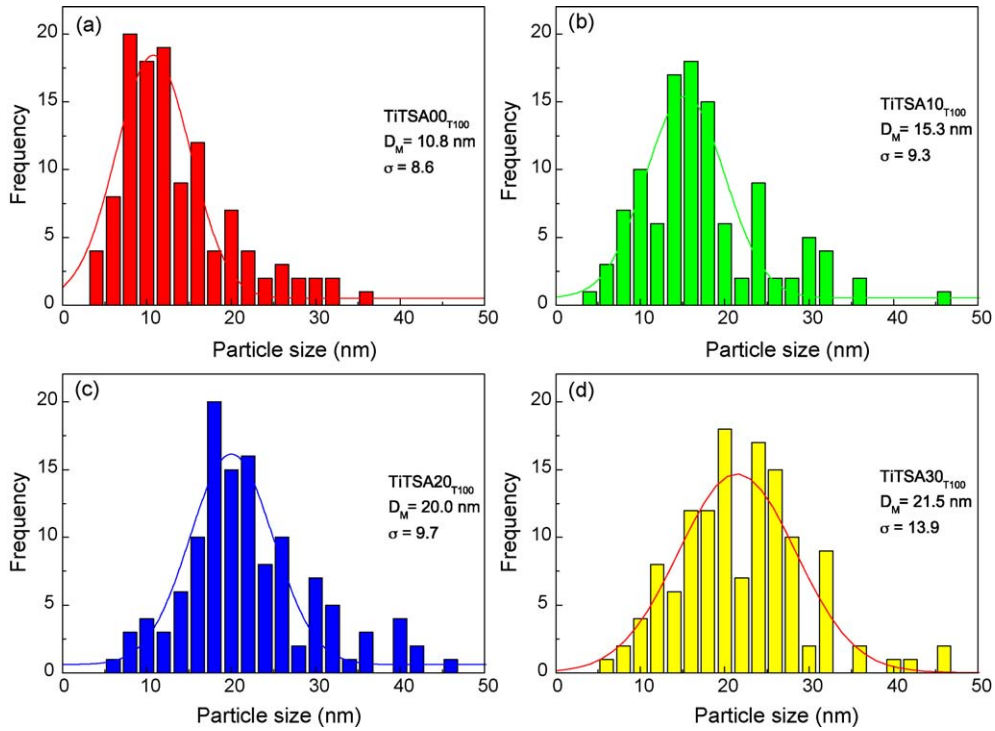

Fig. 2. Particle size distribution histograms based on TEM images of $TiTSA00_{T100}$ (a), $TiTSA10_{T100}$ (b), $TiTSA20_{T100}$ (c), and $TiTSA30_{T100}$ (d) samples.

The pH_{PZC} median values of 6.0 and 5.5 were reported for anatase and rutile, respectively [33]. However, this author considers that the pH_{PZC} of titania is rather insensitive to the crystallographic structure, and the value of 5.9 was recommended for both polymorphs. The pH_{PZC} measured for the TiTSA00 sample is in agreement with the values reported in the literature.

The solids without TSA addition presented the highest values of the point of zero charge (Fig. 6) and the pH_{PZC} diminished with the increment of TSA content and the calcination temperature. It decreased slightly with temperature for TiTSA00 and TiTSA10 samples, and more markedly when higher TSA amounts were added. This effect may be attributed to a higher dehydration degree attained when the temperature is raised [34].

With regard to the differential scanning calorimetry results, titania calcined at 100 °C ($TiTSA00_{T100}$ sample) showed two endothermic peaks at 98 and 172 °C (loss of physically adsorbed

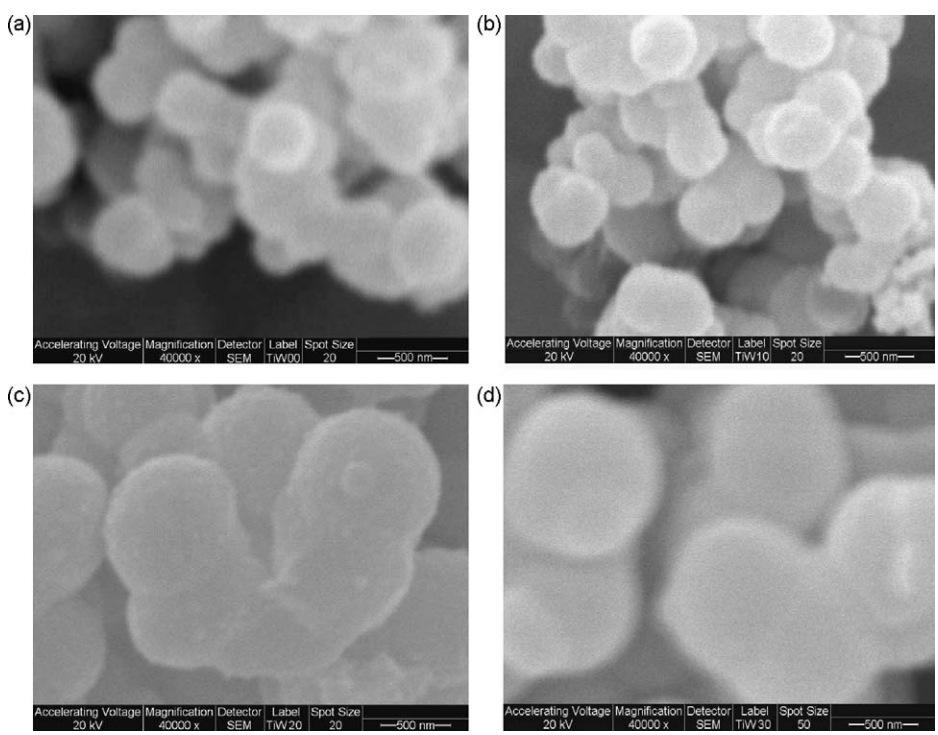

Fig. 3. SEM images of $TiTSA00_{T100}$ (a), $TiTSA10_{T100}$ (b), $TiTSA20_{T100}$ (c), and $TiTSA30_{T100}$ (d) samples (bar size = 500 nm).

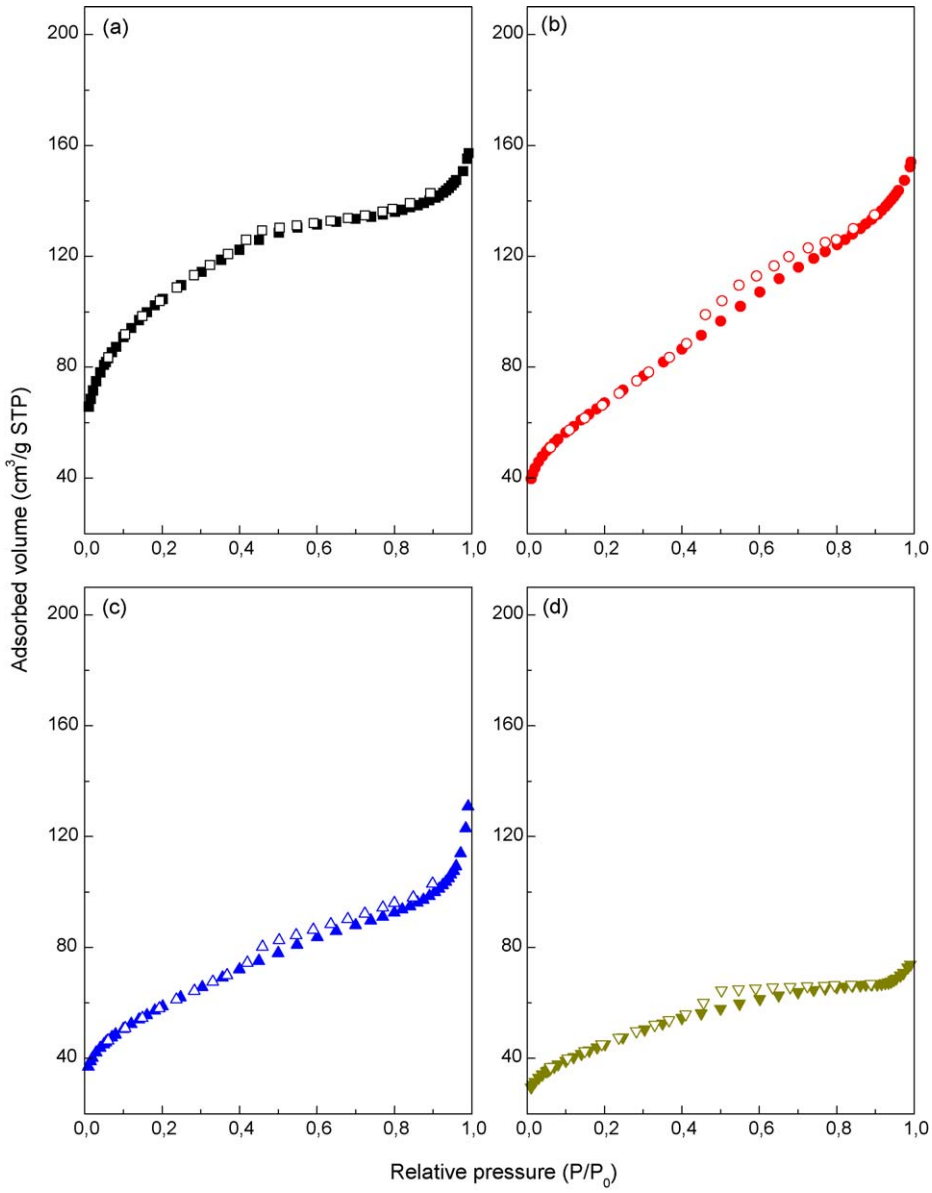

Fig. 4. N_2 adsorption–desorption isotherms of $TiTSA00_{T100}$ (a), $TiTSA10_{T100}$ (b), $TiTSA20_{T100}$ (c), and $TiTSA30_{T100}$ (d) samples. Adsorption branch (full symbols), desorption branch (open symbols).

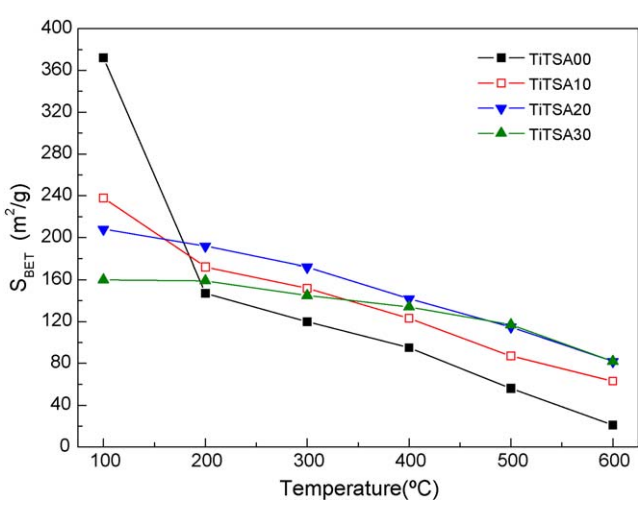

Fig. 5. Variation of S_{BET} as a function of calcination temperature.

and entrapped water [35]), and two exothermic peaks at 408 and 643 °C (anatase phase crystallization [36] and transformation of anatase into rutile phase [37], respectively) in the DSC diagram (Fig. 7a). The very small peak at 324 °C could be assigned to the decomposition of residual organic groups [38–40]. But for the $TiTSA10_{T100}$, $TiTSA20_{T100}$, and $TiTSA30_{T100}$ composites (Fig. 7b–d, respectively) only the endothermic peaks assigned to the physisorbed or entrapped water release were observed.

The observed behavior indicates that there is a delay or an inhibition in the anatase phase crystallization and its transformation into rutile phase, which may be induced by TSA introduction into the titania matrix, similarly to what was reported for tungsten oxide–titania samples [24].

It must be also remarked that the exothermic peak with maximum at 534 °C, assigned to the tungstosilicic anion decomposition, is not present in the DSC diagrams of the TSA/titania samples, while for bulk TSA (Fig. 7e) the peak can be observed together with two endothermic peaks with maxima at 68 and 187 °C, ascribed to the release of physisorbed water and to $H_4SiW_{12}O_{40}{\cdot}6H_2O$ dehydration, respectively [13].

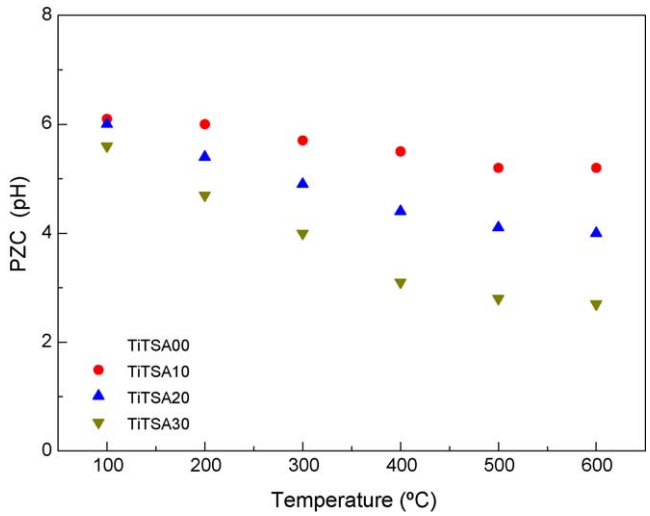

Fig. 6. PZC of TiTSA00, TiTSA10, TiTSA20, and TiTSA30 samples, treated at different temperatures.

On the other hand, two dehydration steps were observed by thermogravimetric analysis of the prepared samples, a loss of physically adsorbed and entrapped water below 200 °C, and a loss of structural or chemically bound water between 200 and 500 °C. According to Munuera et al. [41], two different types of loosely bonded water were completely removed from the surface below 200 °C, and the most tightly bonded one (present on the titania surface in the hydroxyl form) was removed at temperatures higher than 300 °C. From the weight loss in the latter dehydration step, the number of OH groups on the titania surface can be estimated [42]. The number of water molecules released per gram (N_w), in the range 200–500 °C, decreased slightly with the TSA concentration increase in the samples (Table 1). However, the OH group density is less dependent on the TSA content. The estimated values are lower than that of a fully hydroxylated titania powder (12–16 OH/nm^2) [41,43] and higher than that of the commercially available P25 Degussa AG (4.7 OH/nm^2).

It was verified by FT-IR spectroscopy that the urea used as template was completely removed by water extraction of the samples thermally treated at 100 °C, which presented spectra without the more intense characteristic bands of urea, that is, the antisymmetrical and symmetrical stretching vibrations of NH_2 (3439 and 3347 cm^{-1}, respectively) and the stretching vibration of C=O groups (1660 cm^{-1}).

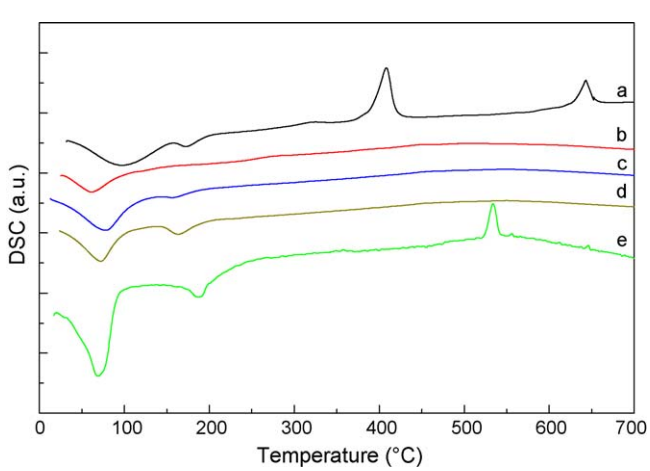

Fig. 7. DSC diagrams of TiTSA00$_{T100}$ (a), TiTSA10$_{T100}$ (b), TiTSA20$_{T100}$ (c), TiTSA30$_{T100}$ (d), and TSA (e) samples.

The spectrum of the TiTSA00$_{T100}$ sample displayed bands with maxima at 3380 (very broad) and 1649 cm^{-1}, assigned to the OH stretching and bending vibrations of water [44] that has been incorporated in the structure [45], and a wide band due to the Ti–O–Ti stretching vibration below 900 cm^{-1} (Fig. 8a). Similar features were observed in the range 1100–4000 cm^{-1} for the TSA/titania composites calcined at 100, 200, 300, 400, and 500 °C, though new bands appeared below 1100 cm^{-1} in these samples with TSA addition, overlapped to the characteristic wide band of titania. The new bands are placed at the same wavenumbers as those of bulk TSA, that is, at 1020, 982, 926, 884, 778, and 541 cm^{-1}, as is observed in Fig. 8 for the samples treated at 100 °C. So, they can be assigned to the $[SiW_{12}O_{40}]^{4-}$ anion. The first band is not assigned, while the others correspond to the stretching vibrations W–Od, Si–Oa, W–Ob–W, W–Oc–W and to the bending vibration Oa–Si–Oa + W–O–W, respectively. The subscripts indicate oxygen bridging the W and the heteroatom (a), corner-sharing oxygen (b) and edge-sharing oxygen (c) belonging to WO_6 octahedra, and terminal oxygen (d). Within the detection limits of FT-IR, it can be established that the Keggin structure of TSA remains unchanged because the main bands of the $[SiW_{11}O_{39}]^{8-}$ lacunar phase placed at 1008, 959, 946, 882, 869, 794, and 720 cm^{-1} (Fig. 8g) were not observed up to 500 °C.

However, when the TSA/titania composites were thermally treated at 600 °C, a decrease of the intensity of the bands assigned to $[SiW_{12}O_{40}]^{4-}$ anion was observed (Fig. 8e), possibly as a result of a partial transformation of the Keggin-type structure.

Finally, the solids were studied by diffuse reflectance spectroscopy. The DRS spectra of the titania without TSA addition showed an intense absorption between 200 and 390 nm, assigned to the charge transfer from the valence band (O 2p) to the conduction band (Ti 3d) [46]. On the other hand, two absorption bands in the range 200–450 nm are shown in the spectrum of bulk TSA [47], attributed to the charge transfer from bridging or terminal O 2p to W 5d (W–O–W and W–O$_d$). For the TSA/titania composites, a charge transfer band shift toward wavelengths near that of bulk

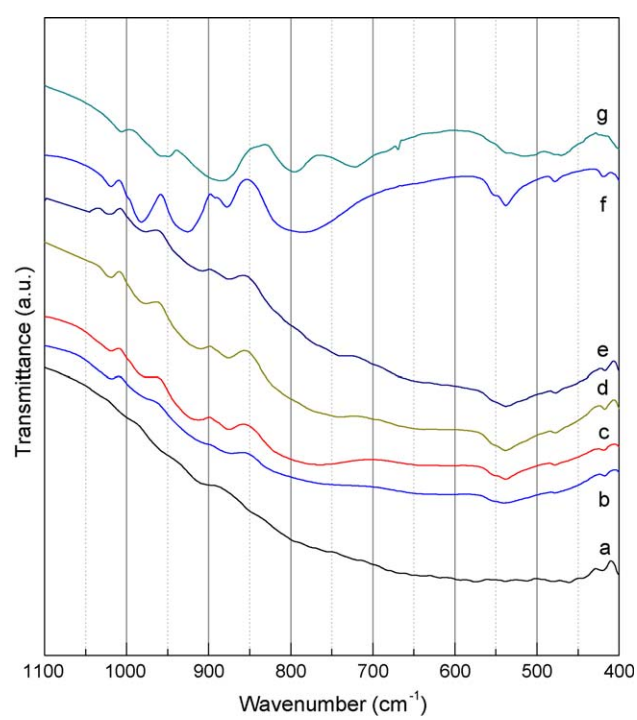

Fig. 8. FT-IR spectra of TiTSA00$_{T100}$ (a), TiTSA10$_{T100}$ (b), TiTSA20$_{T100}$ (c), TiTSA30$_{T100}$ (d), and TiTSA30$_{T600}$ (e) samples; bulk TSA (f), and sodium salt of $[SiW_{11}O_{39}]^{8-}$ anion (g).

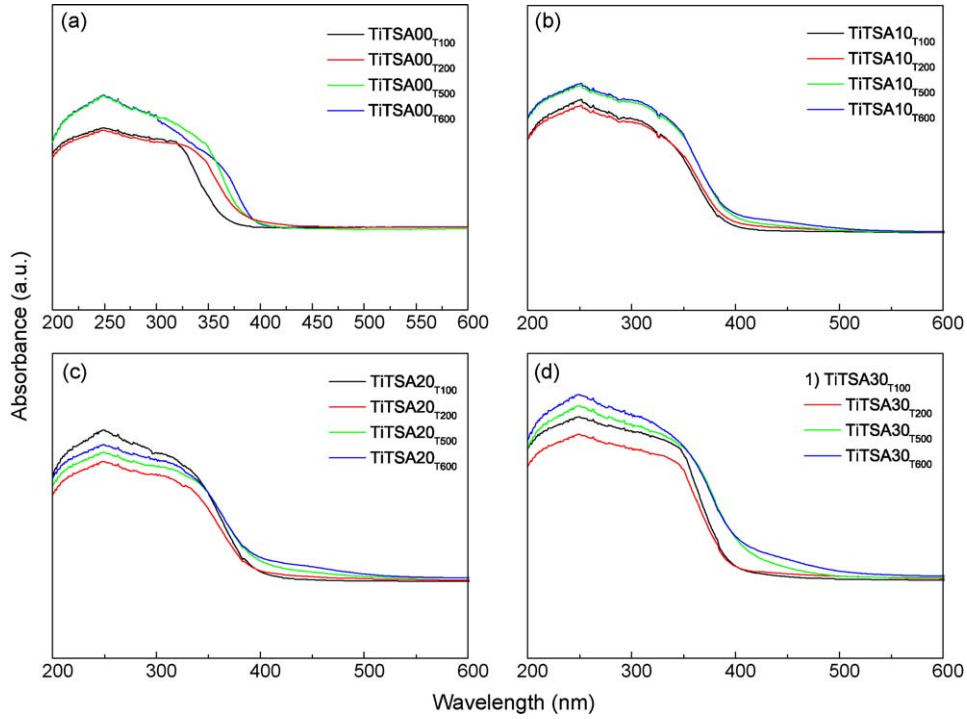

Fig. 9. DRS of TiTSA00 (a), TiTSA10 (b), TiTSA20 (c), and TiTSA30 (d) samples treated at different temperatures.

TSA was observed in the UV–vis DRS spectra, indicating that the tungsten species have an influence on the electronic properties of the samples.

The DRS spectra of the solids thermally treated up to 400 °C showed the absorption threshold onset continuously shifted to the visible region when the TSA concentration increased, as is observed in Fig. 9. However, the red shift of the absorption threshold onset is higher for the samples with TSA addition calcined at 500 and 600 °C.

Taking into account that the Ti 3d and W 5d levels have similar energy, the tungsten addition to anatase should only produce a moderate widening of the electronic bands [46]. The observed red shift of the O → M charge transfer band is indicative of the existence of a doping energy level between the conduction and the valence band of titania.

The *band gap* energy (E_g) of the synthesized samples, estimated from the DRS spectra using the Kubelka–Munk remission function [48], is presented in Fig. 10. For the TiTSA00 samples, E_g is in the range 3.20–2.85 eV. The values decreased with the increase in the calcination temperature. This may be caused by a higher crystallinity degree and/or the appearance of the rutile phase.

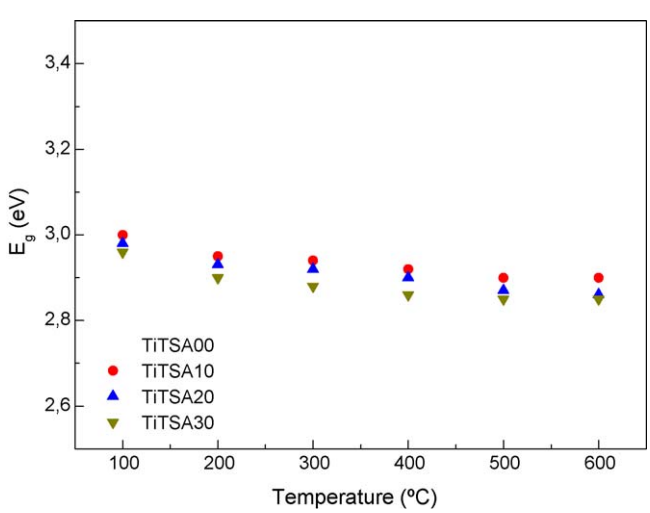

Fig. 10. *Band gap* energy of TiTSA00, TiTSA10, TiTSA20, and TiTSA30 samples calcined at different temperatures.

The *band gap* energy of the TSA/titania composites was lower than that of the TiTSA00 samples as a result of the introduction of TSA in the titania matrix; the order was the following: TiTSA00 > TiTSA10 > TiTSA20 > TiTSA30. However, the decrease was remarkable for the TiTSA10 samples, while the samples with higher TSA concentration exhibited a lower decrease. The E_g values are also lower when the calcination temperature is increased, but they change to a lesser extent than in the case of TiTSA00 sample.

In sum, the TSA/titania composites synthesized by a sol–gel type reaction in only one step, and using urea as low-cost pore-forming agent, lead to mesoporous titania with well-dispersed TSA, and anatase polymorph as the unique titania phase present. In addition, the lower E_g values of titania modified by TSA indicate that it could be possible to use solar light more efficiently than with the unmodified titania.

4. Conclusions

Mesoporous tungstosilicic acid/titania composites were synthesized in only one preparation step, by direct modification of titania gel with TSA, and using urea as a low-cost pore-forming agent.

The obtained samples presented particles with sizes between 200 and 700 nm, which increased for higher TSA concentration and thermal treatment temperature. They are constituted by spherical nanoparticle aggregates of 4–50 nm size. The textural properties of the samples were influenced by both the TSA concentration used during the synthesis and the temperature of the thermal treatment. The specific surface area decreased and the mean pore diameter increased with the TSA concentration and the calcination temperature increase, though a higher specific surface area is obtained for TSA/titania composites compared to unmodified titania. The presence of highly dispersed TSA also retarded the phase transition of anatase into rutile.

The tungstosilicic anion was the main heteropolyoxometallate species present in the composites thermally treated up to 500 °C, and then it could be partially transformed at higher temperature.

Both the addition of TSA to the synthesized titania and the increase of the thermal treatment temperature led to the decrease of the *band gap* energy of the TSA/titania composites.

The preparation method employed allows us to obtain mesoporous TSA/titania composites with interesting properties, such as textural characteristics, the crystalline structure, the crystallite size, the TSA dispersion, which in turn lead to a *band gap* decrease compared to bare titania. The obtained values of these properties are among those that one aims to achieve in the titania-based materials intended to be used as catalysts for pollutant photodegradation.

Acknowledgments

The authors are very grateful to V. Fuchs, E. Soto and L. Osiglio for their experimental contribution, and to CONICET and UNLP for the financial support.

References

[1] A. Sclafani, L. Palmisano, M. Schiavello, J. Phys. Chem. 94 (1990) 829.
[2] K.B. Kyoko, S. Kazuhiro, K. Hitoshi, O. Kiyomi, A. Hironori, Appl. Catal. A: Gen. 165 (1997) 394.
[3] S. Sakulkhaemaruethai, S. Pavasupree, Y. Suzuki, S. Yoshikawa, Mater. Lett. 59 (2005) 2965.
[4] J.-Y. Zheng, J.-B. Pang, K.-Y. Qiu, Y. Wei, Micropor. Mesopor. Mater. 49 (2001) 189.
[5] L.R. Pizzio, Mater. Lett. 59 (2005) 994.
[6] M. Anpo, Catal. Surv. Jpn. 1 (1997) 169.
[7] A. Sclafani, M.N. Mozzanega, P.J. Pichat, Photochem. Photobiol. A: Chem. 59 (1991) 181.
[8] W. Lee, Y.R. Do, K. Dwight, A. Wold, Mater. Res. Bull. 28 (1993) 1127.
[9] T. Carlson, G.L. Griffin, J. Phys. Chem. 90 (1986) 5896.
[10] S. Ikeda, N. Sugiyama, B. Pal, G. Marci, L. Palmisano, H. Noguchi, K. Uosaki, B. Ohtani, Phys. Chem. Chem. Phys. 3 (2001) 267.
[11] A. Fuerte, M.D. Hernández-Alonso, A.J. Maira, A. Martínez-Arias, M. Fernández-García, J.C. Conesa, J. Soria, G. Munuera, J. Catal. 87 (2002) 1.
[12] I.V. Kozhevnikov, Chem. Rev. 98 (1998) 171.
[13] T. Okuhara, N. Mizuno, M. Misono, Adv. Catal. 41 (1996) 221.
[14] E. Papaconstantinou, Chem. Soc. Rev. 18 (1989) 1.
[15] C. Hu, B. Yue, T. Yamase, Appl. Catal. A: Gen. 194–195 (2000) 99.
[16] A. Mylonas, E. Papaconstantinou, J. Mol. Catal. A: Chem. 92 (1994) 261.
[17] L. Li, Q.-Y. Wu, Y.-H. Guo, Ch.-W. Hu, Micropor. Mesopor. Mater. 87 (2005) 1.
[18] R.R. Ozer, J.L. Ferry, Environ. Sci. Technol. 35 (2001) 3242.
[19] M. Yoon, J.A. Chang, Y. Kim, J.R. Choi, K. Kim, S.J. Lee, J. Phys. Chem. B 105 (2001) 2539.
[20] Y. Yang, Y. Guo, C. Hu, Y. Wang, E. Wang, Appl. Catal. A: Gen. 273 (2004) 201.
[21] V.M. Fuchs, E.L. Soto, M.N. Blanco, L.R. Pizzio, J. Colloid Interface Sci. 327 (2008) 403.
[22] J.S. Noh, J.A. Schwarz, J. Colloid Interface Sci. 130 (1988) 157.
[23] X.-F. Yu, N.-Z. Wu, H.-Z. Huang, Y.-C. Xie, Y.-Q. Tang, J. Mater. Chem. 11 (2001) 3337.
[24] H. Yang, D. Zhang, L. Wang, Mater. Lett. 57 (2002) 674.
[25] E. Ortiz-Islas, T. López, R. Gómez, M. Picquart, D.H. Aguilar, P. Quintana, Appl. Surf. Sci. 252 (2005) 853.
[26] D. Carriazo, M. Addamo, G. Marcì, C. Martín, L. Palmisano, V. Rives, Appl. Catal. A: Gen. 356 (2009) 172.
[27] S. Bakardjieva, J. Šubrt, V. Štengl, V. Balek, M.J. Dianez, M.J. Sayagues, Appl. Catal. B: Environ. 58 (2005) 193.
[28] K.M.S. Khalil, T. Baird, M.I. Zaki, A.A. El-Samahy, A.M. Awad, Colloid Surf. A 132 (1998) 31.
[29] N. Phonthammachai, T. Chairassameewong, E. Gulari, A.M. Jamieson, S. Wongkasemjit, Micropor. Mesopor. Mater. 66 (2003) 261.
[30] S. Eibil, B.C. Gates, H. Knozinger, Langmuir 17 (2001) 107.
[31] S.M. Kumbar, G.V. Shanbhag, F. Lefebvre, S.B. Halligudi, J. Mol. Catal. A: Chem. 256 (2006) 125.
[32] F. Lefebvre, J. Chem. Soc., Chem. Commun. (1992) 756.
[33] M. Kosmulski, Adv. Colloid Interface Sci. 99 (2002) 255.
[34] G.A. Parks, Chem. Rev. 65 (1965) 177.
[35] T. López, E. Sánchez, P. Bosch, Y. Meas, R. Gómez, Mater. Chem. Phys. 32 (1992) 141.
[36] K. Yu, J. Zhao, Y. Tian, M. Jiang, X. Ding, Y. Liu, Y. Zhu, Z. Wang, Mater. Lett. 59 (2005) 3563.
[37] J.R. Sohn, J.S. Han, Appl. Catal. A: Gen. 298 (2006) 168.
[38] E.J. Kim, S.H. Hahn, Mater. Sci. Eng. A 303 (2001) 24.
[39] J. Madarász, A. Braileanu, M. Crisan, G. Pokol, J. Anal. Appl. Pyrol. 85 (2009) 549.
[40] H.K. Yu, T.H. Eun, G.R. Yi, S.M. Yang, J. Colloid Interface Sci. 316 (2007) 175.
[41] G. Munuera, V. Rives-Arnau, A. Saucedo, J. Chem. Soc., Faraday Trans. I 75 (1979) 736.
[42] R.M. Mueller, H.K. Kammler, K. Wegner, S.E. Pratsinis, Langmuir 19 (2003) 160.
[43] H.P. Boehm, M. Hermann, Z. Anorg. Allg. Chem. 352 (1967) 156.
[44] J. Rubio, J.L. Otero, M. Villegas, P. Durán, J. Mater. Sci. 32 (1997) 643.
[45] J.A.R. Van Veen, F.T.G. Veltmaat, G. Jonkers, J. Chem. Soc., Chem. Commun. (1985) 1656.
[46] R.D. Shannon, Acta Crystallogr. A 32 (1976) 751.
[47] P.I. Villabrille, L.R. Pizzio, P.G. Vázquez, C.V. Cáceres, M.N. Blanco, Curr. Top. Colloid Interface Sci. 6 (2003) 43.
[48] S.P. Tandom, J.P. Gupta, Phys. Stat. Sol. 38 (1970) 363.